ORIGINAL PAPER: SOL-GEL AND HYBRID MATERIALS FOR OPTICAL, PHOTONIC AND OPTOELECTRONIC APPLICATIONS

Effect of Forster resonance energy transfer on the photoluminescence of PPy-ZnO composite

Smita Dey [1] · Asit Kumar Kar[1]

Abstract

The structural and optical properties of polypyrrole-ZnO (PPy-ZnO) composites with different amount of ZnO are investigated. The nature of optical absorption and emission of the composites having agglomerated granular morphology is explored. Addition of ZnO slightly affects the conjugation of the polymer chain due to which the π-π* transition of PPy-ZnO composite shows some blue shift in the UV-Vis absorption spectra. The photoluminescence intensity of PPy-ZnO nanocomposite varies with variation of ZnO content. This tunability in the photoluminescence intensity of PPy-ZnO nanocomposite can be understood in terms of Forster Resonance Energy transfer (FRET) from ZnO (donor) to PPy (acceptor). The energy transfer efficiency, Forster radius and separation between donor and acceptor are predicted theoretically by using a FRET model. With the change in donor concentration, the energy transfer efficiency changes which affects the emission intensity of composites. The highest emission intensity is observed for 1.22 g of ZnO which indicates the highest energy transfer between ZnO and PPy. Thus, by tuning ZnO content the emission properties of the PPy-ZnO composite can be tuned.

Graphical Abstract
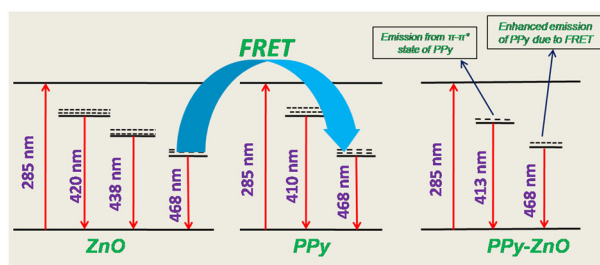
Highlights
- Semiconducting PPy-ZnO composites are synthesised here with different amount of ZnO.
- Enhanced photoluminescence is obtained in composite as compared to pristine PPy.
- FRET from ZnO to PPy is responsible for the PL enhancement.
- Blue emission from all the composites is observed.

✉ Smita Dey
    smita.click@gmail.com

[1] Micro and Nanoscience Lab, Department of Physics, Indian
    Institute of Technology (Indian School of Mines),
    Dhanbad, Jharkhand, India

1 Introduction

Composites of conducting polymer and metal oxide attract the attention of the scientific community due to the synergetic properties of both the components. When a conducting

conjugate polymer interacts with an inorganic metal oxide, different types of photo physical interactions such as charge transfer and Forster resonance energy transfer (FRET) take place in between polymer chain and metal oxide which control the luminescence of the composite. The process of energy transfer between the two materials can tune the emission range of the composite as well as the emission intensity. The composites of conducting polymer and metal oxide have several applications in the field of light emitting diodes [1, 2] and solar cells [3, 4]. For the purpose of applications, it is very necessary to identify the interactions between the polymer and the inorganic material. Several papers focus on the detailed study of the above interactions for various hybrids organic-inorganic composite materials on the basis of optical properties such as absorbance and photoluminescence (PL) spectra. Selmarten [5] et al. explained the photoluminescence quenching of InP quantum dots by conjugated polymer on the basis of a charge transfer mechanism. In case of polymer-metal oxide nanocomposite due to type II band alignment, a charge transfer mechanism occurs; this quenches the photoluminescence intensity. In spite of charge transfer, there is a possibility of energy transfer in the composite which can enhance the overall emission intensity of the composite to some extent. The condition for the energy transfer in the composite is the overlapping of the absorbance spectrum of the acceptor with the emission spectrum of the donor. Lutich [6] et al. reported that in spite of the possibility of charge transfer mechanisms, there is an energy transfer mechanism between PDFD polymer and CdTe nanocrystals due to the superposition of the absorbance spectra of CdTe and the emission spectra of PDFD.

Conducting polymers such as polyaniline (PAni) and polypyrrole (PPy) are very important because of their high electrical conductivity, environmental and thermal stability. ZnO is an inorganic metal oxide semiconductor with wide band gap of 3.32 eV. The visible emission of ZnO depends upon different defect states such as oxygen vacancy, zinc vacancy, zinc interstitial sites, etc. Since PPy is a non-fluorescent polymer, it cannot be used as an emissive layer of PLEDs or for any display applications. But there is a possibility of having luminescence from the composite of PPy-ZnO due to the presence of ZnO which is luminescent. Several works have focussed on PPy-ZnO nanocomposite for the application of solar cell [7], photocatalysis [8, 9], sensors [10–12] etc. But very few papers discussed the possibility of enhancement of the photoluminescence in the composite and the interactions behind the luminescence behaviour of the composite material. There is a type II band alignment between PPy and ZnO which causes the charge transfer. However, the spectral overlap of the absorbance spectrum of PPy with the emission spectrum of ZnO brings the possibility of FRET from ZnO to PPy. This can result in enhanced PL intensity of the composite.

In this work the ZnO concentration dependent optical and structural properties of PPy-ZnO composites are studied. The enhanced emission intensity of the PL emission spectra of PPy-ZnO composite is discussed using a Forster resonance energy transfer mechanism. Several parameters such as geometry of donor and acceptor, concentration of donor or acceptor, separation between donor and acceptor dipoles are responsible for FRET between the two molecules. In the case of the PPy-ZnO composite, PPy is acceptor and ZnO is donor. Here donor concentration is varied for the synthesis of the composite. The energy transfer efficiency, Forster radius, separation between PPy and ZnO are predicted using donor concentration dependent FRET theory.

2 Experimental

2.1 Materials used

Zinc acetate, sodium hydroxide, ethanol and ammonium peroxydisulphate (APS) were purchased from Merck. Pyrrole was purchased from Sisco research laboratory.

2.2 Synthesis of ZnO

Zinc acetate was used as a precursor for the synthesis of ZnO due to its high solubility and low decomposition temperature [13]. Here, 10.1 g zinc acetate was mixed with 50 ml ethanol and stirred until it dissolved. In a separate beaker, 2 g of NaOH was mixed with 50 ml of ethanol and stirred to dissolve. Afterward both solutions were mixed together and heated at 60 °C for 6 h to obtain a white precipitation which was separated by filtration and dried at room temperature. Hence, ZnO nanoparticles in powder form were obtained by the sol gel method.

2.3 Synthesis of polypyrrole-ZnO composites

A chemical oxidative polymerisation method was employed for the synthesis of PPy-ZnO composites in the presence of ZnO particles. Here, 0.3 M pyrrole solution was prepared by adding 1 ml of pyrrole (density = 0.96 g/ml) in a mixed solvent of 48.7 ml of DI water and 0.3 ml of H_2SO_4. Then, 0.8 g of ZnO was mixed with the pyrrole solution and the mixture was stirred for 30 min to enable the pyrrole monomers to adsorb on the surface of ZnO. A 0.37 M APS solution was prepared by dissolving 4.22 g of APS in a mixed solvent of 48.7 ml of DI water and 0.3 ml of H_2SO_4. After 30 min, the APS solution was added drop wise to the solution of pyrrole to start the polymerisation process under continuous stirring. The whole solution was stirred for another 30 min and kept for 24 h under static conditions for

completion of the polymerisation process. A black precipitate was formed which was extracted through filtration and dried at 60 °C to obtain PPy-ZnO composite in powder form (labelled as PZ2).

Following a similar process as discussed above, two more composites were synthesised by varying the ZnO amount (1.22 and 1.68 g, labelled as PZ3 and PZ4, respectively).

2.4 Characterisation methods

Microstructural feature of the samples was obtained by scanning electron microscopy (Supra 55, Carl Zeiss, Germany). The crystalline structure of the samples was obtained by X-ray diffraction (PANalytical Xpert Pro MPD) using Cu K_α radiation. A UV-Vis spectrophotometer (Agilent Cary 5000) was used to obtain the absorbance spectra of the samples in the range of 200 to 800 nm. Photoluminescence emission spectra were recorded using a lifetime spectrometer (Horiba Acton 2500) at the excitation wavelength of 285 nm. Photocatalytic experiment was done in a closed chamber containing a UV lamp (Power = 8W, emission wavelength = 365 nm) to check the degradation performance of PZ3 for the degradation of methylene blue dye.

3 Results and discussion

3.1 Crystallinity of PPy-ZnO composites: XRD pattern

The XRD pattern of PPy as well as PPy-ZnO composites are shown in Fig. 1.

All the PPy-ZnO composites as well as pure PPy shows a broad peak centred at about $2\theta = 23°$. This indicates the amorphous nature of PPy and PPy-ZnO composite. In the case of composites, ZnO particles are fully covered by PPy chains during the oxidative polymerisation of pyrrole in the
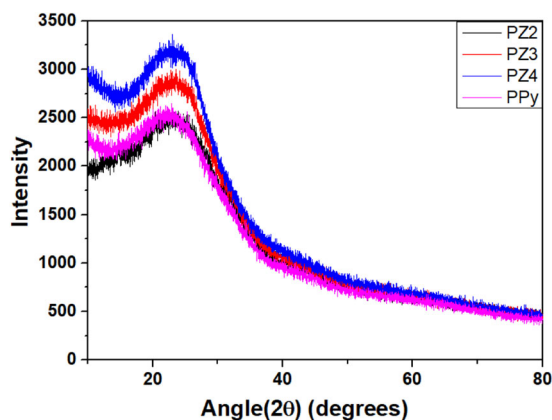

Fig. 1 XRD pattern of PPy and PPy-ZnO composites.

presence of ZnO. Hence, no peak is observed in the XRD powder patterns corresponding to ZnO. The intensity of the peak at 23° increases with increase in ZnO concentration, consistent with an interaction between PPy and ZnO in the composite.

3.2 Microstructural features: SEM

The surface morphology of PPy-ZnO composites as well as pure PPy and ZnO are shown in Fig. 2.

A rock like ZnO structure is observed, whereas PPy possesses spherical granular particles which are interconnected with each other giving rise to agglomerated network like features. PPy-ZnO composites also show similar features to PPy. The particle size of PPy is smaller in the case of composites as compared to pristine PPy. When PPy is synthesised in the presence of ZnO particles, it can be assumed that ZnO particles are well covered by PPy chains in the composites. The size of the PPy granules also varies with the ZnO amount in the composite. The particle size of PZ3 is lowest among the three composites. This may be due to changes in the local environment during polymerisation of pyrrole in the composite with varying ZnO content. It is also observed that PPy particles are more densely distributed in the composites as compared to pristine PPy.

4 Optical properties

4.1 Absorbance spectroscopy

The absorbance spectrum of ZnO is shown in Fig. 3 whereas those of PPy and PPy-ZnO composites are shown in Fig. 4.

The peaks at 370 and 590 nm are related to the π-π* transition and polaron band transition of PPy, respectively. A blue shift of the π-π* transition of PPy in the composites is observed. This validates the interaction of PPy and ZnO in the PPy-ZnO composite. The blue shift is due to the overall decrease in the conjugation length of the polymer chain [14]. This occurs due to bending or twisting of the polymer chain due to the introduction of ZnO in the PPy matrix. The absorbance spectra of composites are the sum over the absorbance of PPy and ZnO. No additional absorbance peak is observed for the composites. This indicates that no ground state charge transfer occurs in the composites [15]. Again, in the case of the composites, the peak due to polaron band transition of PPy is suppressed with the addition of ZnO. The tauc plot for the calculation of band gap of ZnO was shown in the inset of Fig. 3, whereas the band gaps of all the composites and pristine PPy were calculated using Tauc plot as shown in Fig. 5.

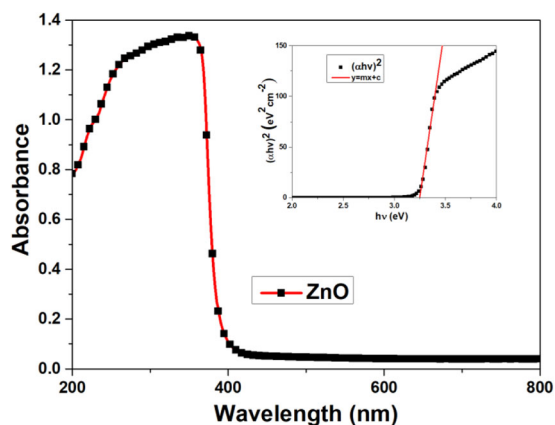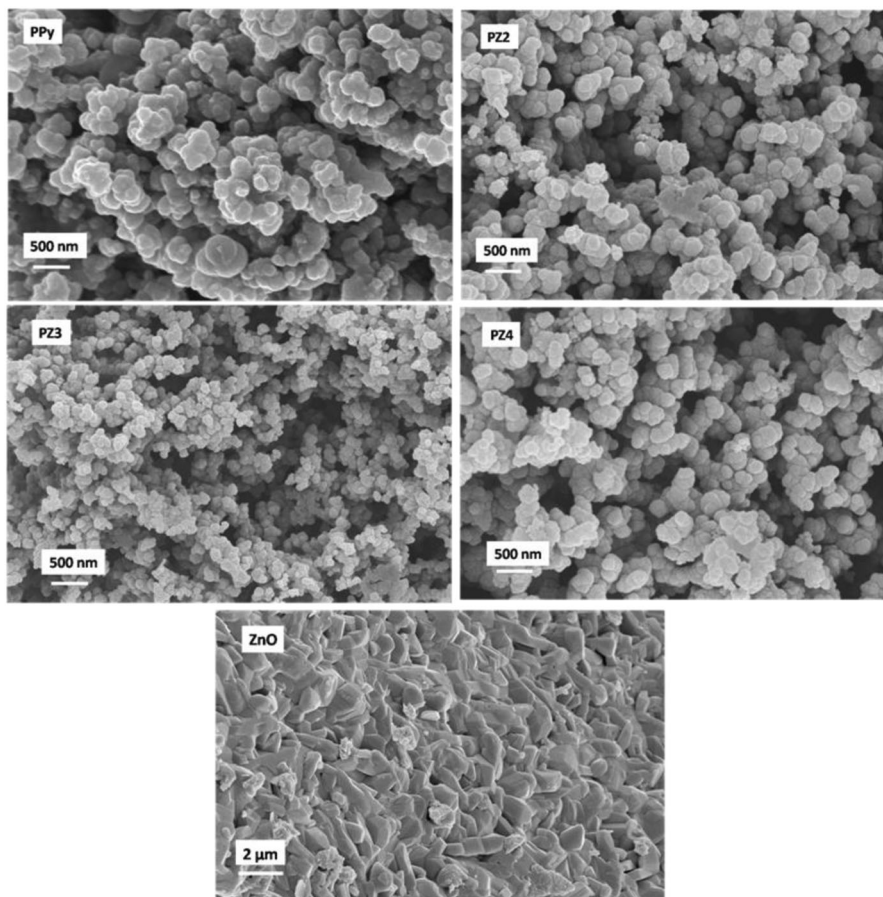Fig. 2 SEM micrographs of PPy, PPy-ZnO composites (PZ2, PZ3 and PZ4) and ZnO.

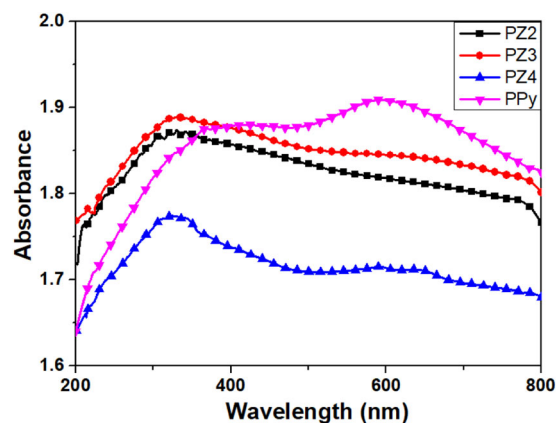Fig. 3 UV-Vis absorbance spectrum of ZnO (inset: Tauc plot of ZnO).

Fig. 4 UV-Vis absorbance spectra of PPy and PPy-ZnO composites.

The band gap values are listed in Table 1.

The band gap of PPy-ZnO nanocomposite increases as compared to pure PPy. The presence of ZnO generates some disorder in the polymer chains, which leads to variations in the band gap of the composite as compared to pristine PPy. The degree of disorder in the polymer chains varies with variations of ZnO content in the composites, thus resulting in a variation in their band gap.

4.2 Photoluminescence spectra of PPy-ZnO composite

Figure 6 presents the PL spectra of pristine PPy and ZnO while Fig. 7 presents the PL spectra of all PPy/ZnO composites.

PPy has two emission peaks at about 410 and 468 nm. ZnO shows a sharp emission peak at about 438 nm which
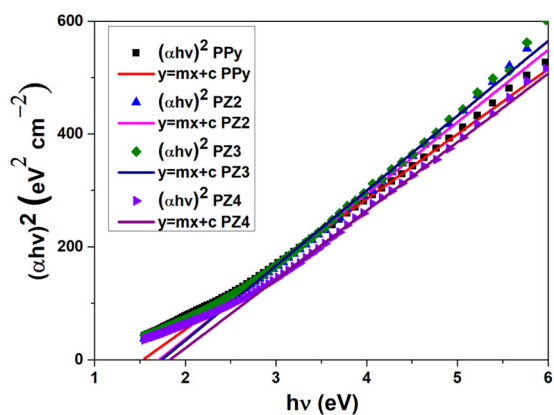
Fig. 5 Tauc plots for the determination of band gaps of PPy and PPy-ZnO nancomposites.
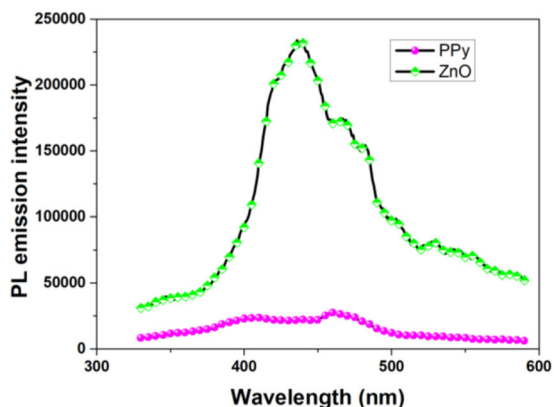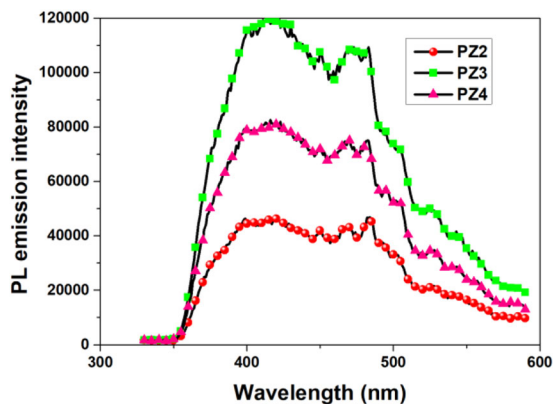

Fig. 6 PL emission spectra of PPy and ZnO.

Fig. 7 PL emission spectra of PPy-ZnO composites.

Table 1 Values of band gap.

Samples	ZnO	PPy	PZ2	PZ3	PZ4
Band gap (eV)	3.25	1.58	1.71	1.74	1.83

arises due to zinc interstitial defects along with two low intensity peaks at about 420 and 468 nm. PPy-ZnO composites exhibit two emission peaks at about 413 and 468 nm. The intensity of the emission peaks changes with the change of ZnO amount in the composite but the peak positions remain the same. Though the emission intensity of PPy is very low, the PPy-ZnO composites shows stronger emission intensity. The emission intensity of the composite increases with increasing ZnO concentration up to a critical concentration of ZnO and after that the intensity falls in spite of higher amount of ZnO.

4.3 Forster energy transfer mechanism behind the enhanced emission of PPy-ZnO composite compared to PPy

FRET is the most probable mechanism that can take place between PPy and ZnO and becomes responsible for the enhanced emission in the composite system as compared to PPy. The spectral overlap in the absorbance spectrum of PPy and emission spectrum of ZnO, as shown in Fig. 8, is an important condition for FRET occurring. The mechanism of FRET in the composite system is shown in the schematic diagram presented in Fig. 9. The details of the FRET mechanism occurring in the system are explained below.

The energy transfer efficiency E with the assumption that a single donor interacts with a single acceptor is written as [16]

$$E = \frac{R_0^6}{R_0^6 + R^6} \tag{1}$$

here R denotes actual separation of the donor and acceptor. The Forster radius R_0 gives the separation between donor and acceptor dipole at which 50% of energy is transferred between donor and acceptor.
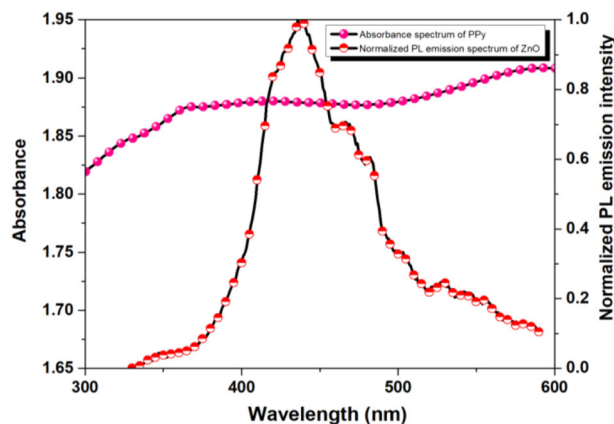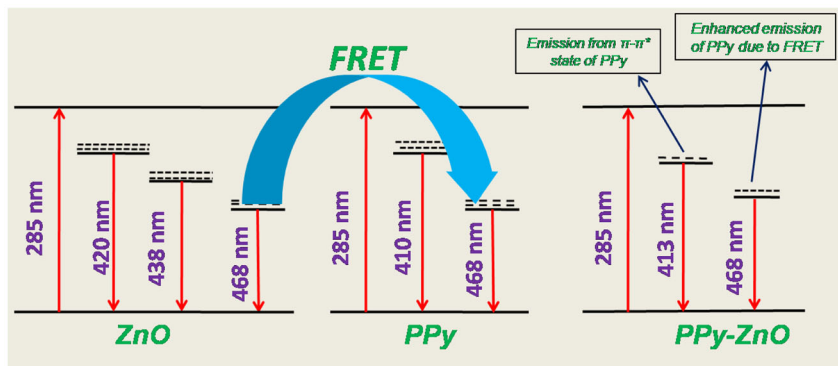

Fig. 8 Spectral overlap between absorption spectrum of PPy and emission spectrum of ZnO.

Fig. 9 Schematic energy level diagram for PPy-ZnO nanocomposite representing FRET in PPy-ZnO composite.

E can be calculated in two ways, either from the quenching of donor emission or enhancement of acceptor emission. Donor emission can be quenched in several ways along with FRET. However, the acceptor emission enhancement can occur only through FRET. So, here the FRET efficiency (E) is determined with the help of Eq. (2) below considering the enhanced acceptor emission.

$$E = \left(\frac{I_{AD}}{I_A} - 1\right)\left(\frac{\varepsilon_A}{\varepsilon_D}\right) \tag{2}$$

here the extinction coefficients of the acceptor and donor at the excitation wavelength of the donor are represented by ε_A and ε_D, respectively. I_{AD} and I_A denote the normalised emission intensity of the acceptor in the presence and absence of the donor, respectively. The values of E obtained from Eq. 2 for PZ2, PZ3 and PZ4 are 0.47, 0.4 and 0.41, respectively. The expression for R_0 is

$$R_0 = 0.0211 \left(\kappa^2 \times \eta^{-4} \times \varphi_D \times J\right)^{\frac{1}{6}} \text{nm} \tag{3}$$

where κ^2 is the orientation factor of the acceptor and donor dipole, η is the refractive index of the medium, and φ_D is the quantum yield of the donor.

The overlap integral J is given by Eq. (4)

$$J = \int I_D(\lambda)\varepsilon_A(\lambda)\,\lambda^4 d\lambda \tag{4}$$

where I_D is the normalised emission spectrum of the donor and ε_A is the extinction coefficient spectrum of the acceptor.

In ZnO-concentration-dependent PPy-ZnO nanocomposites, the assumption of interaction between single donor with single acceptor is invalid. The PL emission intensity of the composites is highly dependent on the concentration of ZnO, which is consistent with a variation in the energy transfer efficiency with the variation of donor (ZnO) concentration. So, it can be assumed that a single donor interacts with multiple acceptors or a single acceptor interacts with multiple donors. Here we assume that a single donor interacts with multiple donors by introducing a new term n in Eq. 1; the modified E is shown in Eq. 5 [17].

$$E = \frac{nR_0^6}{nR_0^6 + R^6} \tag{5}$$

Equation 5 is valid for inter donor-acceptor FRET. Here n denotes the number of acceptors per donor. The value of n can be determined from the ratio of the amount of acceptor to donors using the consideration that the distribution of donor and acceptor is dependent on their amount.

Now consider a new term μ denoting the ratio of R to R_0.

$$\mu = \frac{R}{R_0} \tag{6}$$

Equations (5) and (6) gives the relation shown below

$$\mu^6 = \frac{R^6}{R_0^6} = n\frac{1 - E}{E} \tag{7}$$

here n for PZ2, PZ3 and PZ4 as 1.25, 0.82 and 0.6, respectively. The values of μ for PZ2, PZ3 and PZ4 are calculated as 1.06, 1.03 and 0.9, respectively, from the E value obtained from Eq. 2.

The value of J obtained from Eq. 4 is 7.3×10^{15}. Again, considering the value of κ^2 for random orientations of acceptor and donor dipole as 2/3, η as 2.03 [18] and φ_D of donor (ZnO) as 0.122 [19], the value of R_0 for the PPy-ZnO composite system is 3.8 nm. The values of R for PZ2, PZ3 and PZ4 are obtained as 4.03, 3.9 and 3.7 nm, respectively.

According to concentration-independent FRET theory (Eq. 5), the E value of PZ2, PZ3 and PZ4 are obtained as 0.4, 0.46 and 0.54, respectively, by using the above calculated values of R_0 and R. The energy transfer efficiency for PZ3 is higher than that of PZ2 and it is also found from the PL emission spectra that the emission intensity of PZ2 is higher than that of PZ1. Although the theoretical value of E for PZ4 is highest, experimentally it is observed that the emission intensity of PZ4 is lower than that of PZ3. This occurs due to another phenomenon called donor-donor

FRET. In the case of PZ3, the amount of ZnO (donor) is much higher than that of PPy (acceptor). Hence, the intra-donor FRET is dominant over donor-acceptor FRET, due to which the FRET efficiency decreases for PZ3. The above FRET model is applicable for donor-acceptor FRET. The FRET Eq. (5) fails to explain donor-donor FRET.

4.4 Intradonor FRET

To explain the intradonor FRET, the FRET efficiency equation is modified [20] and written as follows

$$E_{FRET} = \frac{k_{FRET}}{\tau_D^{-1} + k_{FRET}} \tag{8}$$

$$\tau_D^{-1} = k_r + k_{nr} + k_{D-D} \tag{9}$$

here, k_{FRET} denotes the FRET rate. τ_D^{-1} is the decay rate of the donor in the absence of acceptor, k_r and k_{nr} represents radiative and non-radiative transition rates, respectively, and k_{D-D} represents the decay rate due to donor–donor interactions. For higher donor–donor interaction at higher amounts of donor, the value of k_{D-D} becomes significant, which in turn increases the value of τ_D^{-1}. Again, from Eq. (8), it is clear that the higher the value of τ_D^{-1}, the lower will be the E value. Hence, the energy transfer efficiency in PZ4 is less than that of PZ3. It can be also understood that at higher concentrations of donor, concentration dependent inter donor-acceptor FRET theory cannot determine the energy transfer efficiency and separation distance between donor and acceptor in a composite. This is because the concentration-dependent FRET theory is applicable for inter donor-acceptor FRET. But at higher concentration of donor, the intra donor FRET becomes more significant than the inter donor-acceptor FRET. Hence, the energy transfer efficiency of PZ4 calculated using concentration-dependent FRET theory is not the correct result. The exact energy transfer efficiency of PZ4 can be calculated from the time decay data, which is not discussed here.

The FRET parameters for PZ2 and PZ3 are in Table 2.

4.5 Charge separation at the interface of PPy and ZnO: experimental evidence through photocatalysis

PPy and ZnO exhibit type II band alignment which facilitates the charge separation at the interface between the two.

However, from the PL spectra of the composites it is observed that all the composites show higher emission intensity as compared to bare PPy. So, it can be concluded that in spite of having the possibility of charge separation at the interface between PPy and ZnO, charge recombination is observed from the PL spectra. This may be due to the lack of low interfacial interaction between PPy and ZnO. Again, from the absorbance spectra, a blue shift of the π-π* transition of PPy is observed which indicates a decrease in conjugation of the polymer chain. This lowers singlet exciton diffusion through the polymer chain, which ultimately causes the radiative recombination of the exciton before reaching the interface between PPy and ZnO. Hence, the possibility of charge separation decreases. The photocatalysis of PZ3 for the degradation of methylene blue is performed for obtaining experimental evidence of low charge separation in the PPy-ZnO nanocomposite. The photocatalytic experiment was performed for 120 min under UV light. However, the absorbance value of methylene blue at 0 min and at 120 min show only very small difference as shown in Fig. 10. This indicates that no significant degradation of the dye occurs in the presence of PZ3. This occurs due to less charge separation between PPy and ZnO.

4.6 Chromaticity diagram

Figure 11 shows the 1931 CIE chromaticity plot of PPy-ZnO composites.

The CIE coordinates, colour purity and correlated colour temperature (CCT) of the samples are summarised in Table 3.
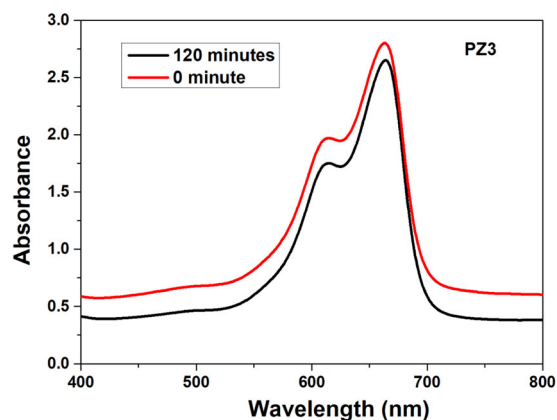

Fig. 10 Time dependent UV-Vis absorbance spectra of methylene blue in the presence of PZ3.

Table 2 Calculated FRET parameters for PZ2 and PZ3.

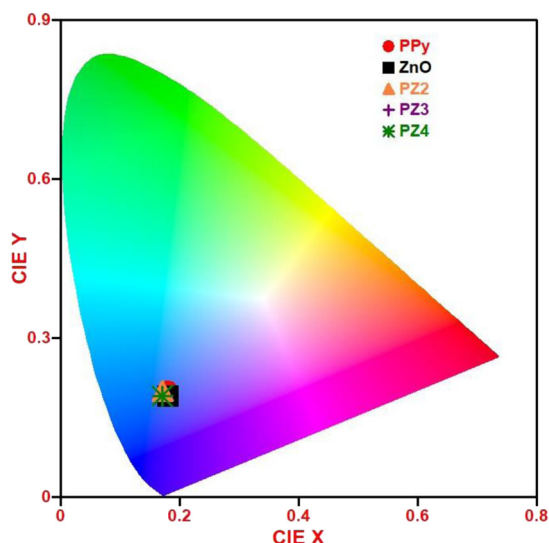| Sample	Forster Radius (R_0) nm	Actual separation between acceptor and donor (R) (nm)	Energy transfer efficiency (E) (%)
PZ2	3.8	4.03	40
PZ3	3.8	3.9	46

Fig. 11 CIE plot of all the samples.

Table 3 CIE coordinates, colour purity and CCT values of all the samples

Samples	CIE coordinates (x, y)	Colour purity (%)	CCT (K)
PPy	(0.18, 0.2)	64	>10,000
ZnO	(0.18, 0.19)	63.1	>10,000
PZ2	(0.17, 0.21)	64.8	>10,000
PZ3	(0.17, 0.19)	68	>10,000
PZ4	(0.17, 0.19)	67.4	>10,000

The CIE plot shows the emission of all the composites is in the blue region. The color purity of the composites is higher than that of pristine PPy and ZnO. The colour purity of PZ3 is highest among all the samples. The CCT values of the all the samples are greater than 10,000 K which indicates that the nature of the color is cool.

5 Conclusions

PPy-ZnO nanocomposites were synthesised with varying ZnO content in the PPy matrix. A blue shift of the absorbance peak due to a π-π* transition of PPy in the composites indicates a decrease in conjugation length in the polymer chain. This decreases the singlet exciton diffusion and facilitates the radiative recombination of the exciton leading to enhanced PL intensity in the composite. The spectral overlap of the absorbance spectrum of PPy and emission spectrum of ZnO indicates the possibility of FRET between PPy and ZnO, although type II band alignment exists among PPy and ZnO. Hence FRET is the most probable reason for the enhanced emission of the composite. The effect of donor (i.e. ZnO) concentration on FRET is also observed from the variations in emission intensity of the PL spectra of PPy-ZnO composites. The dominant intra donor FRET over inter donor-acceptor decreases the overall emission intensity of the composite having higher amounts of ZnO. Hence, tunable photoluminescence through the optimisation of ZnO content in the PPy-ZnO composite makes the composite system a promising candidate for applications in optoelectronic devices.

Compliance with ethical standards

Conflict of interest There is no conflict of interest to declare. The data that support the findings of this study are available from the corresponding author upon reasonable request.

Publisher's note Springer Nature remains neutral with regard to jurisdictional claims in published maps and institutional affiliations.

References

1. Dabbousi BO, Bawendi MG, Onitsuka O, Rubner MF (1995) Electroluminescence from CdSe quantum-dot/polymer composites. Appl Phys Lett 66(11):1316–1318
2. Tessler N, Medvedev V, Kazes M, Kan S, Banin U (2002) Efficient near-infrared polymer nanocrystal light-emitting diodes. Science 295(5559):1506–1508
3. Huynh WU, Dittmer JJ, Alivisatos AP (2002) Hybrid nanorod-polymer solar cells. Science 295(5564):2425–2427
4. Peiró AM, Ravirajan P, Govender K, Boyle DS, O'Brien P, Bradley DD, Durrant JR (2006) Hybrid polymer/metal oxide solar cells based on ZnO columnar structures. J Mater Chem 16(21):2088–2096
5. Selmarten D, Jones M, Rumbles G, Yu P, Nedeljkovic J, Shaheen S (2005) Quenching of semiconductor quantum dot photoluminescence by a π-conjugated polymer. J Phys Chem B 109 (33):15927–15932
6. Lutich AA, Jiang G, Susha AS, Rogach AL, Stefani FD, Feldmann J (2009) Energy transfer versus charge separation in type-ii hybrid organic− inorganic nanocomposites. Nano Lett 9(7):2636–2640
7. Chatterjee S, Shit A, Nandi AK (2013) Nanochannel morphology of polypyrrole–ZnO nanocomposites towards dye sensitized solar cell application. J Mater Chem A 1(39):12302–12309
8. Patil P, Gaikwad G, Patil DR, Naik J (2016) Synthesis of 1-D ZnO nanorods and polypyrrole/1-D ZnO nanocomposites for photocatalysis and gas sensor applications. Bull Mater Sci 39(3):655–665
9. Yan B, Wang Y, Jiang X, Liu K, Guo L (2017) Flexible photocatalytic composite film of ZnO-microrods/polypyrrole. ACS Appl Mater Interfaces 9(34):29113–29119
10. Chougule MA, Dalavi DS, Mali S, Patil PS, Moholkar AV, Agawane GL, Patil VB (2012) Novel method for fabrication of room temperature polypyrrole–ZnO nanocomposite NO2 sensor. Measurement 45(8):1989–1996
11. Barkade SS, Pinjari DV, Singh AK, Gogate PR, Naik JB, Sonawane SH, Pandit AB (2013) Ultrasound assisted miniemulsion polymerization for preparation of polypyrrole–zinc oxide (PPy/

ZnO) functional latex for liquefied petroleum gas sensing. Ind Eng Chem Res 52(23):7704–7712

12. Harpale K, Kolhe P, Bankar P, Khare R, Patil S, Maiti N, Sonawane KM (2020) Multifunctional characteristics of polypyrrole-zinc oxide (PPy-ZnO) nanocomposite: field emission investigations and gas sensing application. Synth Met 269:116542

13. Yang Y, Chen H, Zhao B, Bao X (2004) Size control of ZnO nanoparticles via thermal decomposition of zinc acetate coated on organic additives. J Cryst Growth 263(1–4):447–453

14. Chougule MA, Sen S, Patil VB (2012) Facile and efficient route for preparation of polypyrrole-ZnO nanocomposites: microstructural, optical, and charge transport properties. J Appl Polym Sci 125(S1):E541–E547

15. Greenham NC, Peng X, Alivisatos AP (1996) Charge separation and transport in conjugated-polymer/semiconductor-nanocrystal composites studied by photoluminescence quenching and photoconductivity. Phys Rev B 54(24):17628

16. Clegg RM (2006) The history of FRET. In Reviews in Fluorescence 2006. Springer, Boston, MA, p 1–45

17. Haldar KK, Sen T, Patra A (2010) Metal conjugated semiconductor hybrid nanoparticle-based fluorescence resonance energy transfer. J Phys Chem C 114(11):4869–4874

18. Bodurov I, Yovcheva T, Sainov S (2014) Refractive index investigations of nanoparticles dispersed in water. J Phys: Conf Ser 558(Dec):012062

19. Ramasami AK, Ravishankar TN, Nagaraju G, Ramakrishnappa T, Teixeira SR, Balakrishna RG (2017) Gel-combustion-synthesized ZnO nanoparticles for visible light-assisted photocatalytic hydrogen generation. Bull Mater Sci 40(2):345–354

20. Lunz M, Bradley AL, Gerard VA, Byrne SJ, Gun'ko YK, Lesnyak V, Gaponik N (2011) Concentration dependence of Förster resonant energy transfer between donor and acceptor nanocrystal quantum dot layers: effect of donor-donor interactions. Phys Rev B 83(11):115423